Experimental investigation of Gaussian random phase screen model for x-ray diffusers

KEN VIDAR FALCH,[1,*] CARSTEN DETLEFS,[2] MAGNUS SEBASTIAN CHRISTENSEN,[1] DAVID PAGANIN,[3] AND RAGNVALD MATHIESEN[1]

[1]*Department of Physics, Norwegian University of Science and Technology (NTNU), HÃ¿gskoleringen 1, 7491 Trondheim, Norway*
[2]*Experiments Division, European Synchrotron Radiation Facility (ESRF), 71 Avenue des Martyrs, 38000 Grenoble, France*
[3]*School of Physics and Astronomy, Monash University, Wellington Rd, Clayton, Victoria 3800, Australia*
*kenvidarfalch@gmail.com

Abstract: The beam diffusing properties of stacked layers of diffuser material were evaluated experimentally and compared to a Gaussian random phase screen model. The model was found to give promising accuracy in combination with a Lorentzian auto-correlation model. The tail behaviour of the angular scattering distribution as a function of number of diffusing layers was particularly well described by the model, and in the case of an amorphous carbon diffuser, the model could describe the whole of the scattering distribution convincingly.

1. Introduction and motivation

A common problem with the use of coherent x-ray synchrotron radiation for microscopy is speckles induced by defects or dust on optical components such as mirrors, monochromators, lenses, and x-ray windows. In order to mitigate such speckle effects, so-called diffusers are employed to smooth out unwanted interference patterns. Another important application of diffusers is in the deliberate creation of speckles for X-ray Speckle tracking techniques [1–3]. A diffuser typically consists of some short-range ordered material, such as paper, a piece of wood [4], nano-porous beryllium [5] or carbon [6,7], and sveral others [8–10].

While the motivation of removing speckles is sufficient to make research into the topic of x-ray diffusers worthwhile, there is another motivation behind this work, more specific to the topic of hard x-ray transmission microscopy (HXTM). Recent developments in CRL based microscopy have demonstrated that there are benefits to using an illumination scheme where the illumination is focused by a condenser lens into the centre of the objective lens [7], illustrated in Fig. 1. The benefits of such a scheme is primarily related to mitigation of lateral chromatic aberration, but there is also good reason to believe that it has a mitigating effect on field curvature induced by spherical aberration in objective CRLs [7,11]. The working principle of this illumination scheme was demonstrated by comparing it to a non-condensed parallel beam illumination scheme. This however, might justifiably be considered an inappropriate comparison, as the so-called critical illumination scheme is more commonly used in X-ray transmission microscopy (XTM) [12–14]. Critical illumination consists in using a condenser lens to produce a de-magnified image of the source onto the sample. This has the merit of producing a gain in intensity on the sample. The quality of the condenser lens does not need to be particularity good [15], but the numerical aperture of the condenser lens should be approximately the same as that of the objective lens in order to optimize resolution, commonly referred to as aperture matching.

Compared to critical illumination, the scheme put forth in [7] could be criticized for sacrificing both intensity gain and aperture matching. The first point about intensity can under normal circumstances be dismissed by pointing out that for a given field of view, there is a limited amount of gain possible, which is the gain one would achieve by taking the entirety of the

incident beam and distributing it over the field of view, which is easily achieved in the new illumination by selecting an appropriate focal length for the condenser. If a smaller field of view is required, a longer focal length condenser should be used to allow the beam to condense more before arriving at the sample position. The second allegation on the other hand is a more challenging one, and may not be dismissed so easily. The benefits of aperture matching on the spatial resolution of a microscope can be linked to the coherence length of the illumination. To achieve optimal resolution in a transmission microscope, the coherence length should be shorter than the diffraction limited resolution so that there is no visible interference between adjacent features. Aperture matching, in the critical illumination scheme, produces a coherence length that is equal to the diffraction limited resolution. Here we propose that the diffuser placed between the sample and the condenser lens can provide the same effect. This would have the added benefit of providing field of view and coherence length that can be varied independently, which makes the microscope more flexible with regards to design constraints. The challenge, however, is to reliably engineer diffusers with the desired properties. The experiments and theory presented in this work will take steps towards this end.
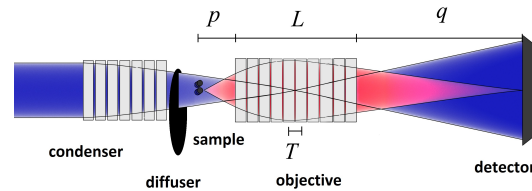

Fig. 1. Sketch of microscope setup.

2. Theory

The model presented here is an extension of the Gaussian random phase screen model [16]. The diffuser is modelled as consisting of n statistically independent diffuser sheets. It is assumed that the sheets are close enough for propagation to be negligible, i.e. the projection approximation is used [17]. The phase shift induced by the diffuser is the sum of contributions from individual layers.

$$\phi(x, y) = \phi_1(x, y) + \phi_2(x, y) \dots \phi_n(x, y). \tag{1}$$

As the phase shift of each individual layer is statistically identical, and statistically independent of the others, the root mean square value (rms) of $\phi(x, y)$, which is denoted by σ_ϕ, is given by

$$\sigma_\phi = \sqrt{n} \cdot \sigma_{\text{layer}}, \tag{2}$$

where σ_{layer} is the rms of the phase shift distribution of a single layer. According to the central limit theorem, the phase distribution $P_\phi(\phi(x, y))$ approaches a Gaussian as n increases

$$p_\phi(\phi) = \frac{e^{-\frac{\phi^2}{2\sigma_\phi^2}}}{\sqrt{2\pi\sigma_\phi^2}}, \tag{3}$$

regardless of the form of the underlying phase distribution of the individual layers. It can be shown [16, 18] that if a plane wave was passed through such a diffuser, the resulting mutual coherence function would be

$$\Gamma(\Delta x, \Delta y) = \langle e^{i\phi(x,y)} e^{-i\phi(x+\Delta x, y+\Delta y)} \rangle = e^{-\sigma_\phi^2 (1 - \gamma_\phi(\Delta x, \Delta y))}, \tag{4}$$

where $\gamma_\phi (\Delta x, \Delta y)$ is the yet unspecified normalized correlation function of $\phi(x, y)$. Note that this result is valid for any value of σ_ϕ, and does not rely on small phase approximation. The power spectral density, $G\left(q_x, q_y\right)$ can be computed by invoking the Wiener-Khinchin theorem, which states that $G\left(q_x, q_y\right)$ is the Fourier transform of $\Gamma(\Delta x, \Delta y)$.

$$G\left(q_x, q_y\right) = \int_\infty^\infty \Gamma(\Delta x, \Delta y)\, e^{iq_x \Delta x + iq_y \Delta y} \mathrm{d}\Delta x \mathrm{d}\Delta y. \tag{5}$$

The mutual coherence function and the power spectral density are convenient tools for analysing the effects the diffuser will have in different situations. Here in particular, the power spectral density is of interest because it can be directly measured experimentally. Suppose the diffuser is placed in a coherent and converging x-ray beam, as illustrated in Fig. 2, at a distance z upstream of the beam focal point, and an imaging detector is placed in the same plane to record the intensity of the resulting distribution. It is possible to calculate the intensity from the generalized Van Cittert-Zernike theorem [19], and the result is

$$I(x', y') \approx \mathrm{FT}\{\Gamma(\Delta x, \Delta y)\}\left(k\frac{x'}{z}, k\frac{y'}{z}\right) = G\left(k\frac{x'}{z}, k\frac{y'}{z}\right) \tag{6}$$

where x' and y' are the coordinates in the transversal plane where the beam comes to a focus, and $I(x', y')$ is the intensity distribution in that plane.
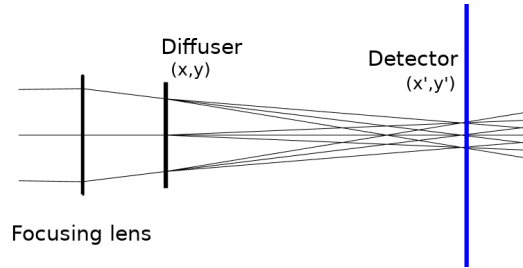

Fig. 2. Illustration of experimental setup.

Here it is assumed that the area of the beam at the diffuser is infinitely large, and would in the absence of a diffuser produce a truly infinitesimally small focal spot, at least within the small angle approximation. In practice, one will not produce such a beam. A real x-ray beam has finite area, partial coherence, both of which will result in a blurring of $I(x', y')$. As the number of layers is increased, σ_ϕ behaves according to Eq. (2), whereas $\gamma_\phi (\Delta x, \Delta y)$ remains unchanged. Following from the central limit theorem, the mutual coherence function should asymptotically approach a Gaussian when n becomes sufficiently large, i.e.

$$\lim_{\sigma_\phi \to \infty} \Gamma(\Delta x, \Delta y) = \lim_{\sigma_\phi \to \infty} e^{-\sigma_\phi^2 \left(1 - \gamma_\phi(\Delta x, \Delta y)\right)} = e^{-\frac{1}{2}(\Delta x^2 + \Delta y^2)\sigma_q^2}, \tag{7}$$

where the value of σ_q scales with σ_ϕ in a way that depends on γ_ϕ. This model has the advantage of not making any assumptions about phase-depth or phase gradient distributions, which allows it to capture an important feature of hard x-ray diffusers, namely the likely existence of a non-scattered fraction of the beam. This point is best illustrated by a demonstration. For this purpose, we use an example that will prove relevant for the experimental results, namely the case of a Lorentzian autocorrelation function,

$$\gamma_\phi (\Delta x, \Delta y) = \frac{1}{1 + (\Delta x^2 + \Delta y^2)/l^2}. \tag{8}$$

Here l is the half width at half maximum value of $(\Delta x^2 + \Delta y^2)$ and can be thought of as transversal coherence length. Figure 3 shows some power spectral densities and mutual coherence functions produced by this model. All the curves were produced using the same γ_ϕ, the only difference between curves is the number of layers, which affects σ_ϕ in accordance with Eq. (2).

Figure 3(a) shows the evolution of the MCF. Initially, at $n = 0$ it is simply 1, as there is no randomness to destroy any correlation. As the number of layers start to increase, we see that a peak appears in the center, on top of a constant background. The value of the background, which is denoted by Γ_∞, can be found by taking the limit in Eq. (4) with Δx going towards infinity.

$$\Gamma_\infty = e^{-\sigma_\phi^2}. \tag{9}$$

Note that this expression holds for any choice of γ_ϕ that tends towards zero at infinity. As the number of layers increase further, Γ_∞ vanishes, and the MCF tends towards a Gaussian shape. With a Lorentzian γ_ϕ, the value of σ_q is given by

$$\sigma_q = \sqrt{2}\frac{\sigma_\phi}{l}. \tag{10}$$

Figure 3(b) shows a logarithmic plot of the power spectral densities calculated from the MCFs. In order to discuss the behaviour of these curves, it is convenient to separate them into two terms that may be thought of as the coherent and the diffuse part.

$$
\begin{align}
G\left(q_x, q_y\right) &= G_0 + G_{\text{diffuse}} \tag{11} \\
G_0\left(q_x, q_y\right) &= \text{FT}\{\Gamma_\infty\}\left(q_x, q_y\right) \propto \Gamma_\infty \delta(q_x, q_y) \tag{12} \\
G_{\text{diffuse}}\left(q_x, q_y\right) &= \text{FT}\{\Gamma(\Delta x, \Delta y) - \Gamma_\infty\}\left(q_x, q_y\right) \tag{13}
\end{align}
$$

One can see from Eq. (12) that the power spectral densities contain a Dirac's delta function due to the non-zero background level, Γ_∞. In the interest of making the figures more presentable, however, the shape has been convoluted by a Gaussian, representing a source with angular rms of $4 \cdot 10^{-6}$ at 17 keV photon energy. This results in an rms value of $3.46 \cdot 10^5$ in q-space. As the number of layers increase, initially, one can see that the central peak is attenuated and eventually disappears as the curve becomes more Gaussian. Figure 3(c) shows a semi logarithmic plot of how the peak attenuates with increasing number of layers. Initially the descent follows the exponential decay law of Eq. (12), but flattens out as the peak amplitude of G_0 becomes small enough to be comparable to the peak of G_{diffuse}. Another property of interest is the width of $G\left(q_x, q_y\right)$. Here it is worth pointing out that $G\left(q_x, q_y\right)$ for different number of layers are related to each other by successive convolutions, i.e.

$$G\left(q_x, q_y; n + m\right) = G\left(q_x, q_y; n\right) * G\left(q_x, q_y; m\right) \tag{14}$$

This is significant because the second order moments of the result of a convolution is the sum of the second order moments of the arguments. This implies that the second order moments of $G\left(q_x, q_y; n\right)$, which is denoted as $\text{rms}_q(n)$, are given by

$$\text{rms}_q(n) = \sqrt{n} \cdot \text{rms}_q(1), \tag{15}$$

which holds, regardless of whether the G_0 peak is present or not. Figure 3(d) demonstrates this fact by showing that the log-log plot of n against $\text{rms}_q(n)$ gives a straight line with a slope of 0.5, indicating a power law relationship with 0.5 as exponent, i.e. a square root relationship.
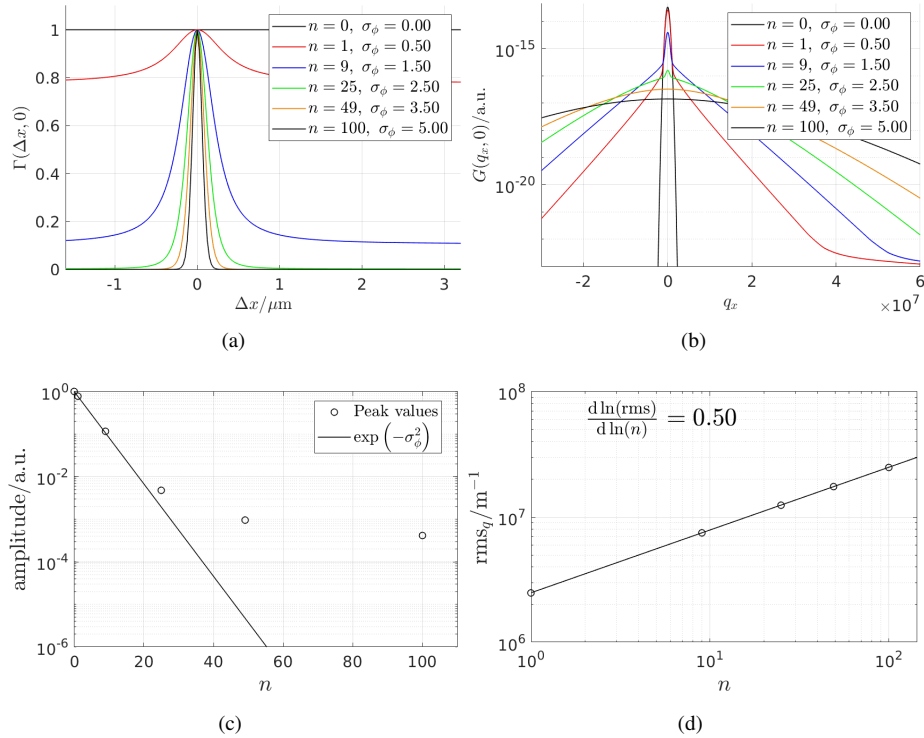
Fig. 3. **(a)** Cross-section of MCF(x, y) according to Eq. (4) calculated for different values of σ_ϕ, using Lorentzian γ_ϕ with $l = 400$ nm. **(b)** cross section of corresponding $G\left(q_x, q_y\right)$ calculated according to Eq. (5), convoluted by a Gaussian with rms $3.46 \cdot 10^5$ m^{-1} in both directions. **(c)** Peak amplitudes of curves in (b). **(d)** Numerically evaluated rms$_q$ of power spectral densities shown in (b).

Consider now the case of a projective imaging system, where a parallel beam passes straight through a sample and the beam is recorded some distance downstream. A diffuser would affects an image from such an imaging system in two important ways. The first by smoothing out unevenness in the illumination, and the second by the blurring of image details. The former depends on how far upstream of the sample the diffuser is placed, while the latter primarily depends on the distance from the sample to the detector. A thorough theoretical description of this topic will be presented by Paganin et al [20] and is not discussed in detail here.

For imaging systems with objective lenses (stigmatic imaging systems), such as a full field microscope, the situation is different. With an objective lens, all rays emerging from a point on the sample plane are focused on a particular point in the image plane, provided the ray passes through the objective lens' aperture. The distance from sample to detector is therefore not directly relevant. What matters instead is the influence of the diffuser on the transmission cross-coefficients (TCC) [21, 22]. The image intensity is given by

$$I\left(\mathbf{r}\right) = \int \mathrm{TCC}(\mathbf{q}', \mathbf{q}'')\tilde{\psi}\left(\mathbf{q}'\right)\tilde{\psi}^*\left(\mathbf{q}''\right)e^{-i(\mathbf{q}'-\mathbf{q}'')\mathbf{r}}\mathrm{d}^2\mathbf{q}'\mathrm{d}^2\mathbf{q}'', \qquad (16)$$

where $\mathbf{r}$ is a two dimensional coordinate vector in the image plane, $\tilde{\psi}$ is the Fourier transform of the wave front perturbation imparted by the sample, and $\mathbf{q}'$ and $\mathbf{q}''$ are two-dimensional

reciprocal coordinate vectors. TCCs is given by

$$\text{TCC}(\mathbf{q'}, \mathbf{q''}) = \int G(\mathbf{q}) P(\mathbf{q'} + \mathbf{q}) P^*(\mathbf{q''} + \mathbf{q}) \, d^2\mathbf{q}, \qquad (17)$$

where P is the pupil function of the imaging system. Unfortunately, computation of $I(\mathbf{r})$ for arbitrary G and P is computationally heavy, as the TCC must be computed over a four-dimensional grid. The problem can be computationally simplified by singular value decomposing $\text{TCC}(\mathbf{q'}, \mathbf{q''})$, known as the sum over coherent systems method [23, 24], but this was not done here. Here we have made due with solving a simplified problem, where the sample is constant along the y-axis. In this case, it follows from the Fourier slice theorem that $\tilde{\psi}$ is non-zero only when $q_y = 0$. One then only has to compute TCC in the two-dimensional sub-space where q'_y and q''_y is zero in order to evaluate $I(\mathbf{r})$ from (16). Figure 4 gives a demonstration of how image resolution is affected by G. Figure 4(a) show the image resolution for a fixed value of l, with varying σ_ϕ, and Fig. 4(b) show a similar case, but with a varying l and constant σ_ϕ. This demonstrates that with Lorentzian $\gamma_\phi(\Delta x, \Delta t)$, both l and σ_ϕ has an impact on resolution.
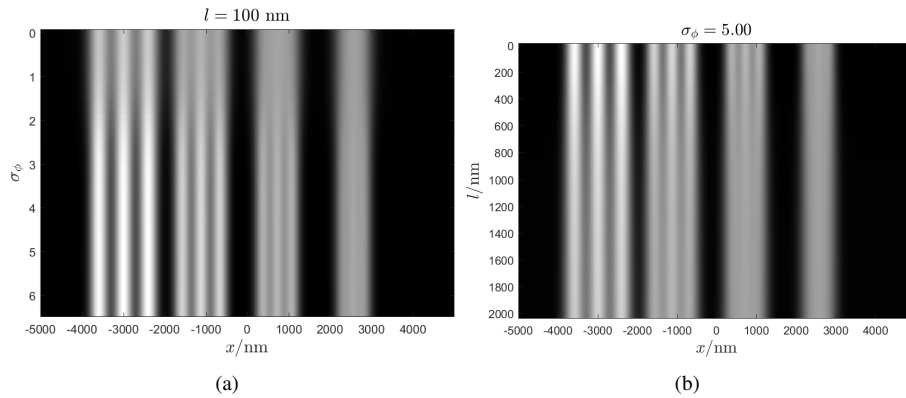

Fig. 4. 1-dimensional simulations of CRL microscopy. The sample were four gratings of size pitch 590 nm, 460 nm, 350 nm and 270 nm. Each horizontal row of pixels represents an individual 1D simulation using the corresponding parameter value on the vertical axis. x is the spatial coordinate. (**a**) Constant l. (**b**) Constant σ_ϕ. The aperture in both cases was a Gaussian window with an angular rms of 6.6×10^{-5}, and the photon energy was 17.2 keV, which results in a diffraction limited resolution of 250 nm.

3. Experimental setup

The experiment was performed at ID06 at ESRF with a setup similar to the one illustrated in Fig. 2. A synchrotron x-ray undulator source was monochromatised to 17 keV by a Si111 double crystal monochromator. A CRL was placed about 50 meters downstream of the source. The CRL consisted of 4 Beryllium lenslets with 50 μm radius of curvature. This casts a focal spot onto a high resolution indirect x-ray imaging detector, about 5.9 m downstream of the CRL. The detector was composed of a scintillator screen (10 μm LuAG:Eu on a 170μm YAG substrate) [25], optical microscope with Olympus UIS2 UPlanSApo 10 × /0.40 objective and Olympus U-TLU-1-2 tube lens. The optical microscope is operated without an eye piece, projecting the intermediate image directly onto an ESRF FreLoN camera [26] with 2000 × 2000 pixels. This combination yields and effective pixel size of 1.4 × 1.4 μm^2 and a field of view of 2.8 × 2.8 mm^2. The thickness of the scintillator screen is a compromise between quantum efficiency (x-ray absorption) and resolution (due to the limited depth of field of the objective). The beam size incident on the CRL was limited by a 200 × 200 μm pair of slits located 1.2 m upstream of the CRL. Due to

geometrical constraints, the camera was positioned only 5.5 m from the CRL. With a numerical aperture of 16.8μ rad, this theoretically results in 15 μm blurring of the source image. The diffuser position was in between the CRL and detector, 4.7 m from the detector. The diffuser consisted of polishing papers made of Al_2O_3 particles on 3 mm thick layers of polyester. The number of diffuser layers, n, was varied systematically. The diffuser was spun with an angular velocity that was fast enough to not give any intensity variations from image to image. Small angle scattering patterns were recorded with different number of layers. In addition, a single disc of amorphous carbon was investigated. This carbon diffuser disc have been used in several CRL-Microscopy experiments in the past [6, 7].

While the theoretical effects of partial coherence on microscopy images are well understood, it is of interest to observe the real impact with actual diffusers in actual microscopes. In order to do so, a full field microscope was set up in the same beamline. A sketch of the Microscope can be seen in Fig. 1. The objective lens consisted of 89 Be lenslets with 50μm radius of curvature with an average spacing along the optical axis of T=1.7 mm, resulting in a focal length of 190 mm measured from the entrance of the lens stack. The condenser lens consisted of 32 Be lenslets of the same type, with a T =2 mm spacing along the optical axis, yielding a focal length of about 640 mm. The distance between sample and objective lens entrance was $p = 210$ mm, the length of the objective lens was $L = 148$ mm, and the distance between objective lens exit and detector was $q = 4000$ mm, yielding an x-ray magnification of 14. The detector was the same FReLoN camera used in the small angle scattering experiment. The effective pixel size, taking x-ray magnification into account, was measured to be 88 nm. The diffuser was placed approximately 170 mm from the sample.

4. Results

Figure 5 shows a semi-logarithmic plot of the collected scattering data. It is evident that curve broadens as the number of layers increase. It also appears that the tails of curves make straight lines in the logarithmic plot, which implies that the tails decay exponentially. We note that this phenomena appears to be present even at $n = 1$, where the phase-depth presumably was small. This is significant because at shallow phase-depth,

$$\Gamma\left(\Delta x, \Delta y\right) \approx \left(1 - \sigma_\phi^2\right) + \sigma_\phi^2 \gamma\left(\Delta x, \Delta y\right). \tag{18}$$

The curves, according to Eq. (6), are measurements of the Fourier transform of $\Gamma\left(\Delta x, \Delta y\right)$. As the constant term in Eq. (18) does not contribute to the tails of the Fourier transform, the exponential tails stem from γ_ϕ, i.e. the Fourier transform of γ_ϕ have exponential tails. A simple function that behaves in this way is the Lorentzian function. This can be seen in Fig. 3(b), particularly in the curve for $n = 1$. The Fourier transform of a Lorentzian is a symmetrical, two-sided sided, exponential function (Laplacian distribution). We therefore attempted to model the data using a Lorentzian phase-correlation function.

Simulated curves were produced by first choosing a value of l and phase depth for a single layer, σ_{layer}. Then, for every n, σ_ϕ was set to $\sigma_{layer}\sqrt{n}$. From this, $\Gamma\left(\Delta x, \Delta y\right)$ could be determined according to Eq. (4), allowing $G\left(q_x, q_y\right)$ to be calculated from Eq. (5). To simulate scattering patterns, an image of the focal spot, recorded without any layers, was convoluted by $G\left(q_x, q_y\right)$. The displayed curves are cross-sections of the resulting scattering patterns. The results can be seen in the dashed lines in Fig. 5. The tail behaviour seem to scale appropriately with n. Note that only two parameters, namely $l = 2.3\mu$m and the phase depth for a single layer, taken to be 0.65 , was used to produce all of the curves. Near the origin, however, there are notable discrepancies suggesting that γ_ϕ was not truly a Lorentzian. We speculate that scattering from the 3 mm thick polyester film which the Al_2O_3 particles were attached to might play a role in this. Figure 6 shows the result of applying the same procedure to the scattering data from the

carbon diffuser disc. The model here produced a convincing match to the experimental data. The Lorentzian model appears to be an excellent fit for this diffuser.
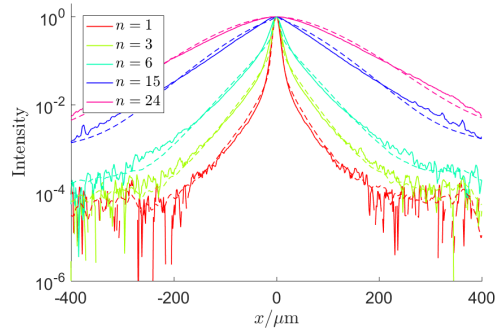

Fig. 5. Semi-logarithmic plot of recorded small angle scattering pattern. The intensity was rescaled so as to be equal to 1 at the origin. Note the tendency for constant slope away from the origin, suggesting that the tails decay exponentially. The modelling parametres used were $l = 2.3\mu m$, and $\sigma_\phi = 0.65\sqrt{n}$.
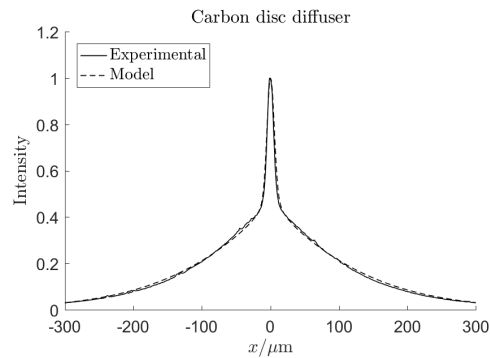

Fig. 6. Small angle scattering pattern produced by carbon disc diffuser and corresponding model fit. The modelling parametres used were $l = 1.1\ \mu m$, $\sigma_\phi = 2.27$, and $n = 1$.

Next we wished to investigate the validity of Eq. (15). Figure 7 shows a log-log plot of the measured rms_q against n. The slope of the curve appears to be approximately correct, however, it should be mentioned that the resulting rms values are highly sensitive to the treatment of background noise.
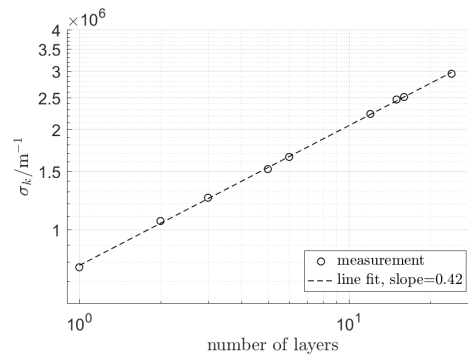
Fig. 7. Root mean square of intensity distribution of scattering patterns produced by layers of sandpaper. The measured slope is highly dependent on the treatment of background noise.

In order to investigate the effects of diffuser on actual CRL microscopy images, a grating with 0.3 μm pitch was placed in the object plane of the microscopy setup and recorded with different number of diffuser layers. The result can be seen in Fig. 8. The first thing that can be observed is that there is the smoothing of the illumination. The large intensity oscillations that are present in most of the field of view in Fig. 8(a) are almost completely removed, even with only 6 diffuser sheets, as seen in Fig. 8(b).

Regarding effects on resolution, the numerical aperture of the objective lens is 3×10^{-4}. The angular distribution of the scattering patterns produced by the diffusers ranged up to approximately 2×10^{-5} rad. Theoretically, based on Eq. (16) and Eq. (17), this angle is much too small to produce an appreciable effect on the resolution. Nevertheless, it is clear that the diffusers are having a significant impact, as can be seen in Fig. 9. It is evident that adding more sheets the shoulder fringes near the absorbing line are attenuated, but so is the depth of the lowest point on the graphs. The observed behaviour is not consistent with the simulation based on Eq. (16) and Eq. (17) as there should not be any shoulder fringes under ideal condition. Conditions are of course not ideal, however, and while it is difficult to identify the cause with high certainty, it seems plausible that the observed effect is a result of interaction between aberration, defocus and partially coherent illumination. We note that significant aberration is known to be present in the type of lenses that were used, but good progress have been made towards corrective optics, which have already been applied in nanofocusing [27]. It is clear that the diffusers have an effect, but it is not obvious which diffuser configuration is better. Assuming lens aberration is in fact the culprit, it is reasonable to expect significant quality improvements with corrective optics, but so far, experiments on full field imaging with corrective optics have not been reported.

It should be noted that in order to bring the angular spread from the diffuser layers to a level closer to the N.A. of the lens, we may extrapolate from Fig. 7 that about 2000 to 3000 layers would be required, suggesting that this particular diffuser material would not be suitable for the purpose of filling the aperture of this objective lens at 17 keV.
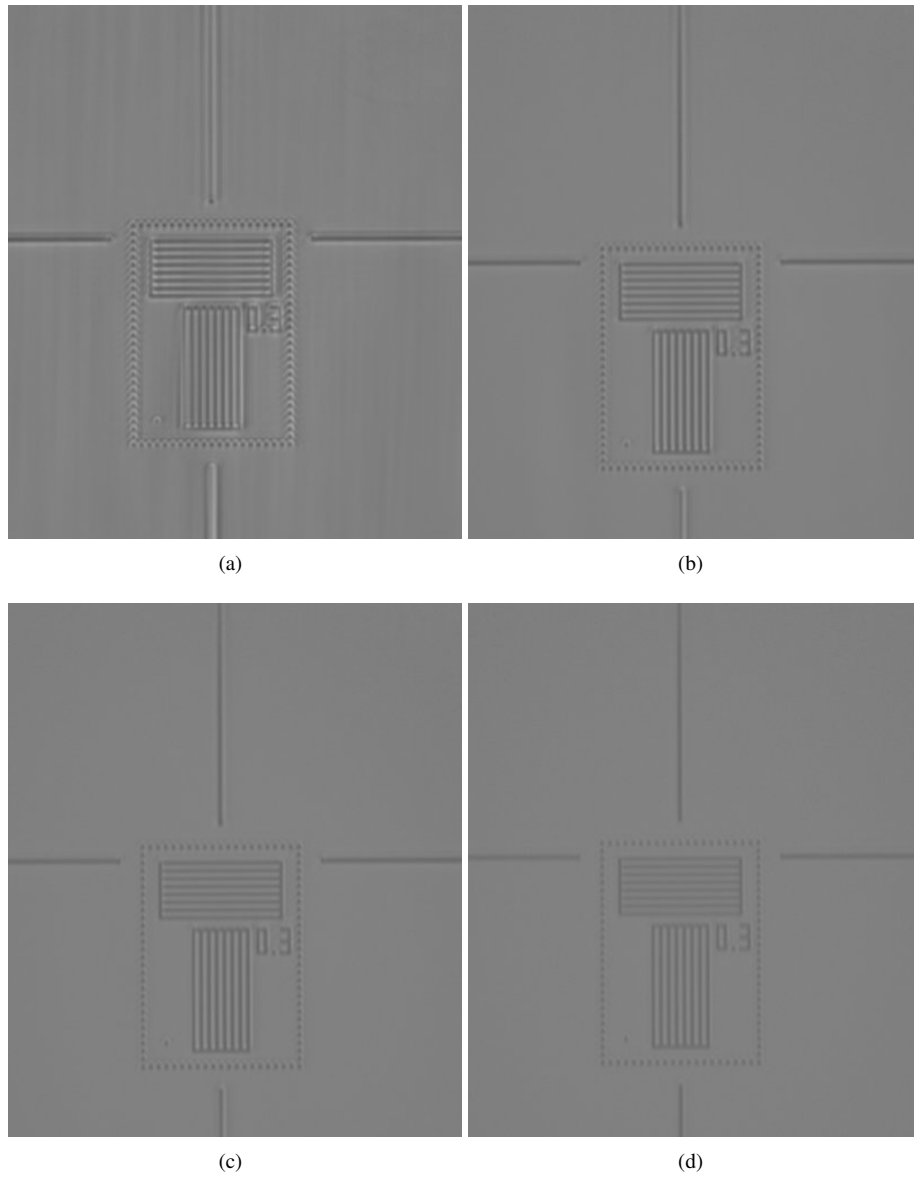
Fig. 8. Microscopy images of 0.3 μm pitch grating, using **(a)** no diffuser, **(b)** 6 layers, **(c)** 12 layers, and **(d)** 24 layers of sandpaper as diffuser.

(a)   (b)
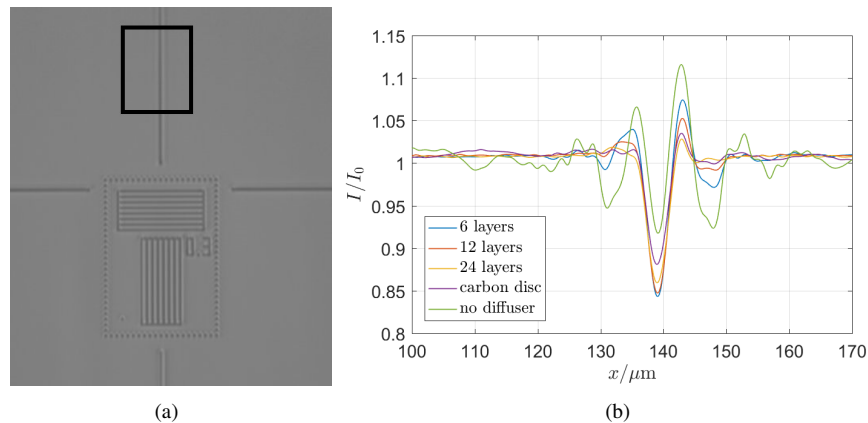
Fig. 9. **(a)** Microscopy image of 0.3 μm pitch grating. **(b)** Vertically averaged intensity profiles sampled from the region indicated by the black rectangle in (a), using varying numbers of diffuser layers.

5. Conclusions

The Gaussian random phase screen model has been identified as a useful theoretical frame work for the design of x-ray diffusers, and can likely be used to evaluate the suitability of a diffuser material quantitatively. The relevant parameters of the model are the phase depth per layer and the auto-correlation function for a single layer. The parameters of the auto-correlation model is independent of number of layers. The model can therefore prescribe how many layers are necessary to achieve the desired quality of illumination. It was shown that a Lorentzian auto-correlation model correctly predicts tail profiles and their behaviour in response to changing number of layers, and in the case of the carbon disc diffuser, it accurately models the full scattering pattern, including the central peak.

Disclosures

The authors declare that there are no conflicts of interest related to this article.

References

1. H. Wang, Y. Kashyap, and K. Sawhney, "From synchrotron radiation to lab source: Advanced speckle-based x-ray imaging using abrasive paper," Sci. Rep. **6**, 20476 (2016).
2. I. A. Aloisio, D. M. Paganin, C. A. Wright, and K. S. Morgan, "Exploring experimental parameter choice for rapid speckle-tracking phase-contrast X-ray imaging with a paper analyzer," J. Synchrotron Radiat. **22**, 1279–1288 (2015).
3. I. Zanette, M.-C. Zdora, T. Zhou, A. Burvall, D. H. Larsson, P. Thibault, H. M. Hertz, and F. Pfeiffer, "X-ray microtomography using correlation of near-field speckles for material characterization," Proc. Natl. Acad. Sci. U.S.A. **112**, 12569–12573 (2015).
4. P. Cloetens, R. Barrett, J. Baruchel, J.-P. Guigay, and M. Schlenker, "Phase objects in synchrotron radiation hard x-ray imaging," J. Phys. D: Appl. Phys. **29**, 133–146 (1996).
5. A. Goikhman, I. Lyatun, P. Ershov, I. Snigireva, P. Wojda, V. Gorlevsky, A. Semenov, M. Sheverdyaev, and A. Snigirev, "Highly porous nanoberyllium for x-ray beam speckle suppression," J. Synchrotron Radiat. pp. 796–800 (2015).
6. K. V. Falch, D. Casari, M. Di Michiel, C. Detlefs, A. Snigireva, I. Snigireva, V. Honkimäki, and R. H. Mathiesen, "In situ hard x-ray transmission microscopy for material science," J. Mater. Sci. **52**, 3497–3507 (2017).
7. K. V. Falch, C. Detlefs, M. Di Michiel, I. Snigireva, A. Snigirev, and R. H. Mathiesen, "Correcting lateral chromatic aberrations in non-monochromatic x-ray microscopy," Appl. Phys. Lett. **109**, 054103 (2016).
8. Y. Matsuura, I. Yoshizaki, and M. Tanaka, "X-ray diffuser," J. Appl. Crystallogr. **37**, 841–842 (2004).
9. K. S. Morgan, S. C. Irvine, Y. Suzuki, K. Uesugi, A. Takeuchi, D. M. Paganin, and K. K. Siu, "Measurement of hard x-ray coherence in the presence of a rotating random-phase-screen diffuser," Opt. Commun. **283**, 216–225 (2010).

10. S. Sanchez, P. E. Ahlberg, K. M. Trinajstic, A. Mirone, and P. Tafforeau, "Three-dimensional synchrotron virtual paleohistology: A new insight into the world of fossil bone microstructures," Microsc. Microanal. **18**, 1095–1105 (2012).
11. K. V. Falch, C. Detlefs, A. Snigirev, and R. H. Mathiesen, "Analytical transmission cross-coefficients for pink beam x-ray microscopy based on compound refractive lenses," Ultramicroscopy **184**, 1–7 (2018).
12. W. Chao, B. D. Harteneck, J. A. Liddle, E. H. Anderson, and D. T. Attwood, "Soft x-ray microscopy at a spatial resolution better than 15 nm," Nature **435**, 1210–1213 (2005).
13. J. C. Andrews, S. Brennan, C. Patty, K. Luening, P. Pianetta, E. Almeida, M. C. H. van der Meulen, M. Feser, J. Gelb, J. Rudati, A. Tkachuk, and W. B. Yun, "A high resolution, hard x-ray bio-imaging facility at SSRL," Synchrotron Radiat. News **21**, 17–26 (2008).
14. B. Kaulich, P. Thibault, A. Gianoncelli, and M. Kiskinova, "Transmission and emission x-ray microscopy: operation modes, contrast mechanisms and applications," J. Physics: Condens. Matter **23**, 083002 (2011).
15. F. Zernike, "The concept of degree of coherence and its application to optical problems," Physica **5**, 785–795 (1938).
16. J. W. Goodman, *Statistical Optics* (John Wiley & Sons, 2015), chap. 8.2.
17. D. Paganin, *Coherent X-Ray Optics* (Oxford University, 2006), chap. 2.
18. M. V. Berry, "Disruption of wavefronts: statistics of dislocations in incoherent gaussian random waves," J. Phys. A: Math. Gen. **11**, 27–37 (1978).
19. J. W. Goodman, *Statistical Optics* (John Wiley & Sons, 2015), chap. 5.8.
20. D. M. Paganin. School of Physics and Astronomy, Monash University, Wellington Rd, Clayton, Victoria 3800, Australia, and A. Mittone, and K. S. Morgan, C. Amendola, K. V. Falch, R. H. Mathiesen, A. Bravin, and Carsten Detlefs are preparing a manuscript to be called "On phase diffusers for phase contrast x-ray imaging".
21. H. H. Hopkins and P. M. Barham, "The influence of the condenser on microscopic resolution," Proc. Phys. Soc. Sect. B **63**, 737–744 (1950).
22. M. Born and E. Wolf, *Principles of Optics* (Pergamon, 1980), chap. 10.
23. Y. C. Pati and T. Kailath, "Phase-shifting masks for microlithography: automated design and mask requirements," J. Opt. Soc. Am. A **11**, 2438–2452 (1994).
24. N. Cobb, "Sum of coherent systems decomposition by SVD," University of California at Berkeley paper (1995).
25. T. Martin and A. Koch, "Recent developments in X-ray imaging with micrometer spatial resolution," J. Synchrotron Radiat. **13**, 180–194 (2006).
26. J.-C. Labiche, O. Mathon, S. Pascarelli, M. A. Newton, G. G. Ferre, C. Curfs, G. Vaughan, A. Homs, and D. F. Carreiras, "Invited article: The fast readout low noise camera as a versatile x-ray detector for time resolved dispersive extended x-ray absorption fine structure and diffraction studies of dynamic problems in materials science, chemistry, and catalysis," Rev. Sci. Instruments **78**, 091301 (2007).
27. F. Seiboth, A. Schropp, M. Scholz, F. Wittwer, C. Rödel, M. Wünsche, T. Ullsperger, S. Nolte, J. Rahomäki, K. Parfeniukas, S. Giakoumidis, U. Vogt, U. Wagner, C. Rau, U. Boesenberg, J. Garrevoet, G. Falkenberg, E. C. Galtier, H. Ja Lee, B. Nagler, and C. G. Schroer, "Perfect x-ray focusing via fitting corrective glasses to aberrated optics," Nat. Commun. **8**, 14623 (2017).